J Mater Sci: Mater Electron (2026) 37:373

Enhanced EMI shielding of Ag–polymer composites via TiB_2 reinforcement in the 2–4 GHz range

Tugay Demirtaş[1,*], Şeyma Atıcı[2,3], Umut Aydemir[2], and Enes Yiğit[2,3]

[1] *Engineering Faculty Electrical and Electronics Engineering, Mudanya University, Bursa 16940, Turkey*
[2] *Engineering Faculty Electrical and Electronics Engineering, Bursa Uludag University, Bursa 16059, Turkey*
[3] *Ulutek Technology Development Zone, FLADRIW Information Technologies Inc., Bursa 16059, Turkey*

Received: 27 October 2025
Accepted: 5 February 2026

ABSTRACT

Due to its exceptional electrical conductivity, high thermal stability, and mechanical hardness, titanium diboride (TiB_2) has emerged as a critical reinforcement material for high performance electromagnetic interference (EMI) shielding. Despite its potential, achieving a synergistic balance between filler dispersion and high shielding efficiency within polymer matrices remains a significant challenge in current research. This study investigates the performance of composite coatings reinforced with TiB_2, a conductive ceramic material, for EMI shielding applications in the 2–4 GHz frequency range. TiB_2 is incorporated into a commercially available Ag polymer at various weight ratios (10–50 wt%), and the resulting composites are evaluated using a Vector Network Analyzer. The reflection (S_{11}) and transmission (S_{21}) parameters are measured to calculate the total shielding effectiveness, which reached a peak of approximately 45 dB at 2.2 GHz. These findings highlight the promise of TiB_2-filled composites as effective EMI shielding materials for use in aerospace, defense, and healthcare applications. Future research will aim to optimize the filler composition and assess material stability under elevated temperatures.

1 Introduction

In the era of 5G communication and Big Data, the rapid proliferation of wireless electronic devices has significantly improved quality of life but has concurrently escalated electromagnetic (EM) radiation pollution, necessitating advanced mitigation strategies [1]. Electromagnetic (EM) waves play a pivotal role in modern communication technologies due to their capability to propagate through free space, enabling efficient long-distance information transfer [2]. With the advancement of knowledge and increasing mechanization, the utilization of various electrical and electronic devices in sectors such as healthcare, military, commerce, and scientific research has grown significantly, reportedly by up to four times in recent decades. The increasing number of electronic devices, along with associated infrastructure such as power supply cables, overhead transmission lines, satellites, vehicles, and broadcast towers (TV/radio), emit EM radiation. Such unintended emissions can interfere with the functioning of nearby electronic systems, leading to EM interference (EMI), which disrupts signal integrity and device performance [3]. In the era of electronic information,

Address correspondence to E-mail: tugay.demirtas@mudanya.edu.tr

https://doi.org/10.1007/s10854-026-16789-w
Published online: 12 February 2026

EM radiation may interfere with the proper functioning of electronic devices in military, industrial, and civilian environments, potentially leading to serious risks for human health and the biosphere [4]. With the rapid development of modern technologies, EM radiation emitted by newly designed electronic systems particularly in the microwave range has become a growing concern, leading to the need for effective shielding solutions to prevent interference and device malfunction [5]. EMI refers to the presence of undesirable radiated signals that may lead to significant performance degradation in electronic systems and devices [6]. EMI shielding involves the application of specific materials designed to block or attenuate EM waves between protected regions and external environments. The effectiveness of such shielding relies primarily on the reflection, absorption, and redirection of EM waves by the shielding medium. Despite their excellent EM wave attenuation capabilities, metals are generally unsuitable for lightweight electronic applications due to their high density, bulkiness, limited corrosion resistance, low ductility, complex processing requirements, and elevated cost [7]. To achieve optimal performance, microwave absorbers are required to possess four key characteristics: thin thickness, low density, wide absorption bandwidth, and high absorption intensity [8]. Although conventional metallic shielding materials exhibit high electrical conductivity, their applicability is limited by drawbacks such as substantial weight, susceptibility to corrosion, and the propensity to generate secondary electromagnetic reflections [9].

Therefore, the development of lightweight, flexible, and cost-effective shielding materials is essential to mitigate EMI while maintaining the regular functionality of electronic devices [10].

EM waves not only cause malfunctions and interferences in nearby electronic equipment but are also associated with adverse health effects such as headaches, insomnia, and fatigue, among others. A widely accepted approach to mitigate the hazards of EM waves is the use of EMI shielding materials that either reflect or absorb the incident radiation. In response to the growing need for lightweight and miniaturized electronic devices, substantial research efforts have focused on developing low-density, easily processable EMI shielding materials [11] . The proliferation of wireless communication systems and high-frequency electronic devices has significantly increased the risk of EMI, which can degrade system performance, compromise signal integrity, and raise safety concerns. To mitigate these effects, the development of materials with effective EM shielding and absorption capabilities has become a major research priority, particularly for applications requiring thermal stability and mechanical robustness.

In dielectric materials, the real part (ϵ') of the complex permittivity indicates the material's ability to store EM energy, whereas the imaginary part (ϵ'') reflects the energy dissipation mechanisms, including conduction and polarization losses [12]. The ratio of the imaginary part to the real part of a material's complex permittivity is referred to as the dielectric loss tangent ($\tan \delta\varepsilon$), which characterizes the energy dissipation capability of dielectric materials. Similarly, the magnetic loss tangent ($\tan \delta\mu$) is defined as the ratio of the imaginary part to the real part of the complex permeability, indicating magnetic energy losses within the material. The loss tangent is a key figure of merit for evaluating the performance of EM absorbing materials, as it quantifies the extent of energy dissipation due to EM wave absorption. In general, materials exhibiting higher dielectric and magnetic loss tangents tend to demonstrate superior EM wave absorption capabilities [13]. When examining EM loss mechanisms, conduction loss, dielectric loss, and magnetic loss are the most prominent contributors. When an EM wave interacts with a material, it can be partially absorbed due to multiple internal reflections resulting from the material's structure and electrical conductivity. To maximize EM attenuation, the material should possess sufficient electrical conductivity and high mobility of charge carriers. However, good electrical conductivity alone is not sufficient criterion for an effective attenuation mechanism [14].

EM shielding materials especially those based on ceramic matrices, are increasingly recognized for their ability to function under extreme conditions. In contrast, ceramic materials such as TiB_2 offer excellent thermal stability and environmental resistance, making them ideal for use in extreme operating conditions where metals fail. Among various ceramic fillers, TiB_2 has emerged as a highly promising candidate due to its combination of excellent electrical conductivity, high thermal stability, and chemical inertness. TiB_2-based ceramic matrix composites have attracted considerable attention in recent years due to their superior properties over monolithic TiB_2 ceramics, including high hardness, excellent wear resistance, and enhanced fracture toughness [15]. TiB_2 as a typical

ultrahigh-temperature ceramic, exhibits a unique combination of high melting point, excellent thermal and chemical stability, and metallic-level electrical conductivity, making it a promising candidate for EMI shielding applications where reflection dominates over absorption mechanisms [16].

Beyond traditional metallic and carbon-based materials, advanced titanium-based compounds have drawn attention due to their tunable electronic properties. For instance, recent research on $Ti_3C_2T_x$ MXene-derived semiconductors has shown that inducing structural defects and optimizing the band structure can lead to superior reflection loss and radar cross-section (RCS) reduction. Unlike pristine titanium oxides which may suffer from low conductivity, materials that exhibit metallic-level electrical conductivity, such as TiB_2 provide a more direct path to high EM attenuation through both reflection and conduction loss mechanisms [17].

In the present study, TiB_2 was incorporated into a heat-resistant industrial paint to produce a ceramic-based EM shielding material designed for operation in the 2–4 GHz frequency range. Combining TiB_2 with heat-resistant polymer matrices or paints not only enhances processability and coating adaptability but also maintains electrical conductivity essential for EMI shielding through reflection. This study systematically investigates the EMI shielding effectiveness of TiB_2-based coatings with varying filler concentrations (10%–50%), aiming to identify the optimal composition for high-performance, thermally stable shielding materials. This study contributes to the development of high-performance EM shielding samples suitable for aerospace, defense, and high-power electronics applications, where thermal durability and lightweight shielding are critical.

2 Material and methods

2.1 Theory of shielding

EMI shielding refers to the reflection and/or absorption of EM waves by materials specifically designed to act as protective barriers, preventing EM radiation from penetrating electronic devices. Such shielding typically involves the use of materials with conductive and/or magnetic properties to effectively block or attenuate unwanted EM signals. Ratio of the incident power or electric field or magnetic field intensities to the transmitted power or electric field or magnetic field intensities respectively when expressed in decibel (dB) is called as shielding effectiveness (SE). Mathematically, SE is represented as given in Eq. (1).

$$SE = 10log\left(\frac{P_i}{P_0}\right) = 20log\left(\frac{E_i}{E_0}\right) = 10log\left(\frac{H_i}{H_0}\right) \quad (1)$$

where P_i, E_i and H_i are the incident power, electric, and magnetic field intensities on the shield respectively, and P_0, E_0 and H_0 are the transmitted power, electric, and magnetic field intensities through the shield material, respectively. A high SE value indicates that minimal EM energy is transmitted through the shielding material. According to the literature, a material with an SE of 20 dB is capable of attenuating approximately 99% of the incident EM radiation [18].

According to the Schelkunoff theory, the total SE for a shielding material is given by Eq. (2)

$$SE = SE_R + SE_M + SE_A \quad (2)$$

The attenuation of EMI from reflection of a material can be calculated using Eq. (3)

$$SE_R(dB) = 10\log(\frac{1}{1-|S11|^2}) \quad (3)$$

Similarly, for SE due to absorption (SEA), the same principles apply where part of the incident wave is absorbed as it propagates through the material, contributing significantly to the overall attenuation of EM radiation, as shown in Eq. (4).

$$SE_A(dB) = 10\log(\frac{1-|S11|^2}{|S21|^2} \quad (4)$$

When an EM wave interacts with a material, three fundamental mechanisms govern the wave–material interaction: reflection, absorption, and transmission. These parameters collectively determine the shielding performance of a material. As illustrated in Fig. 1, these key EM phenomena represent how the incident wave is partially reflected at the surface, partially absorbed within the material, and partially transmitted through it.

The SE of a material can be evaluated using various techniques. Among these, the waveguide method based on plane wave radiation measurements is one of the most widely employed approaches for determining the SE of shielding materials [19].

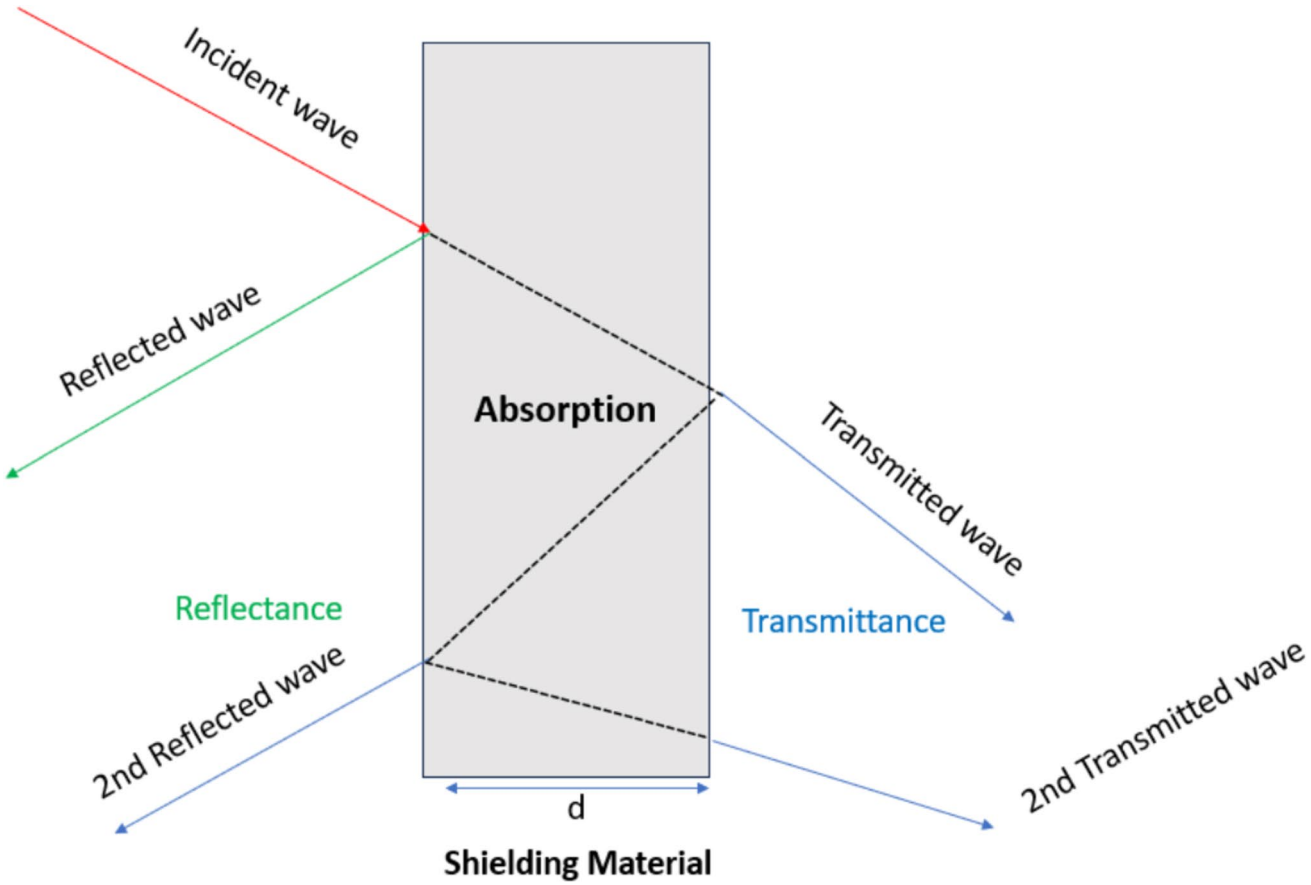

Fig. 1 Interactions of EMI with shielding material

The skin depth (δ) defines the depth at which the EM wave amplitude drops to 1/e of its original value at the surface and is given by Eq. (5). A smaller δ implies higher absorption, which enhances the shielding effectiveness by minimizing internal transmission.

$$\delta = \sqrt{\frac{2}{\mu\sigma w}} = \sqrt{\frac{1}{\pi f \mu\sigma}} \tag{5}$$

In metals with high electrical conductivity, SE is primarily governed by reflection. However, in composite materials, absorption plays a more significant role. In this study, experimental approaches were employed to conduct EM analysis, utilizing the equations provided above to evaluate the material's shielding performance (Fig. 2).

2.2 Experimental setup

The primary material used in this study was titanium diboride (TiB_2), a ceramic material known for its excellent electrical conductivity, high thermal stability, and corrosion resistance. The TiB_2 powder (average particle size: 25 μm) was obtained from Doğuş Döküm Sanayi ve Ticaret A.Ş., İstanbul, Türkiye a commercial supplier of TiB_2 powders (2025). The TiB_2 powder is incorporated into TiB_2-doped Ag polymer composite specifically designed for GHz-frequency applications. The TiB_2-based composite samples are prepared by mixing TiB_2 powder with the industrial heat-resistant paint at a concentration of 10%, 20%, 30%, 40%, and 50%, respectively. After mixing with the specified percentages, the material was poured into polystyrene molds according to the dimensions suitable for the waveguide calibration kit (Fig. 3). After the samples were prepared with the specified molar percentages, they were left to dry in an oven at 40 °C for one day, followed by a further 4 days of self-drying to achieve optimal bonding and uniformity of the coating. The samples were stacked and machined to the dimensions of the calibration kit after being demolded. The EM properties of the prepared samples are characterized

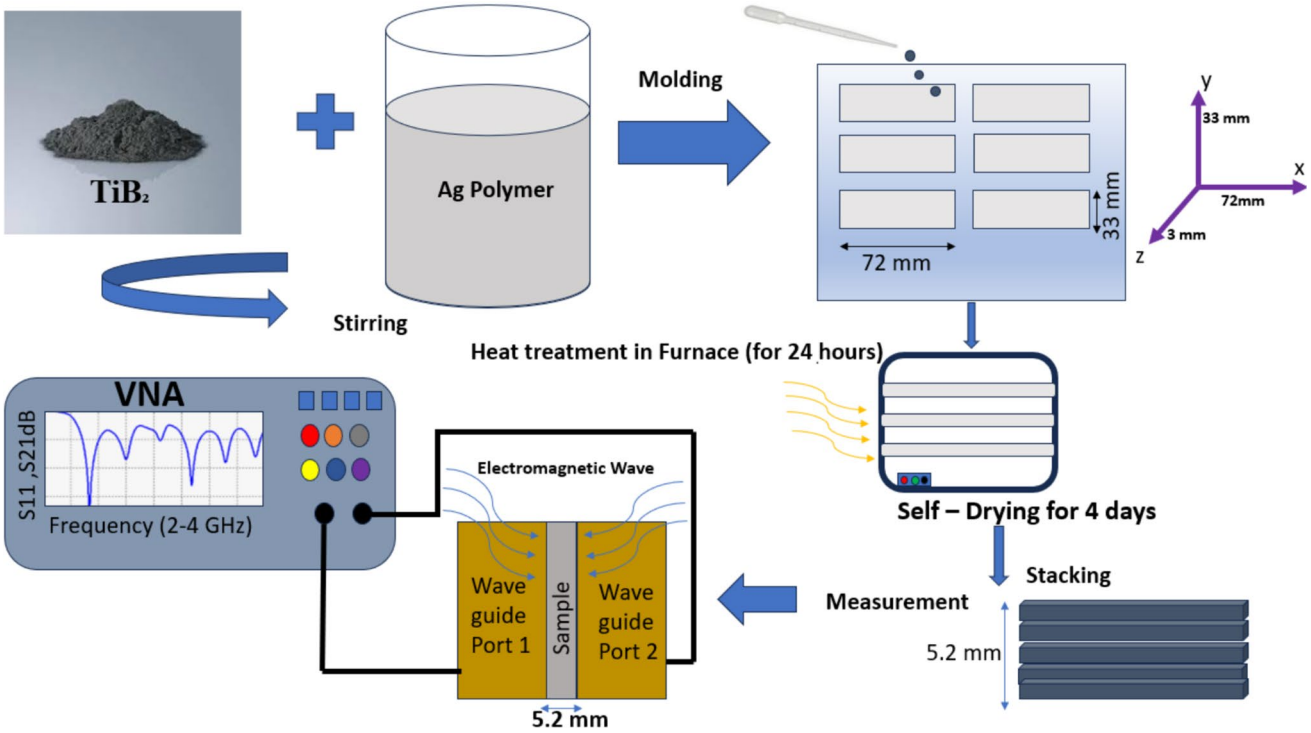

Fig. 2 Experimental scheme

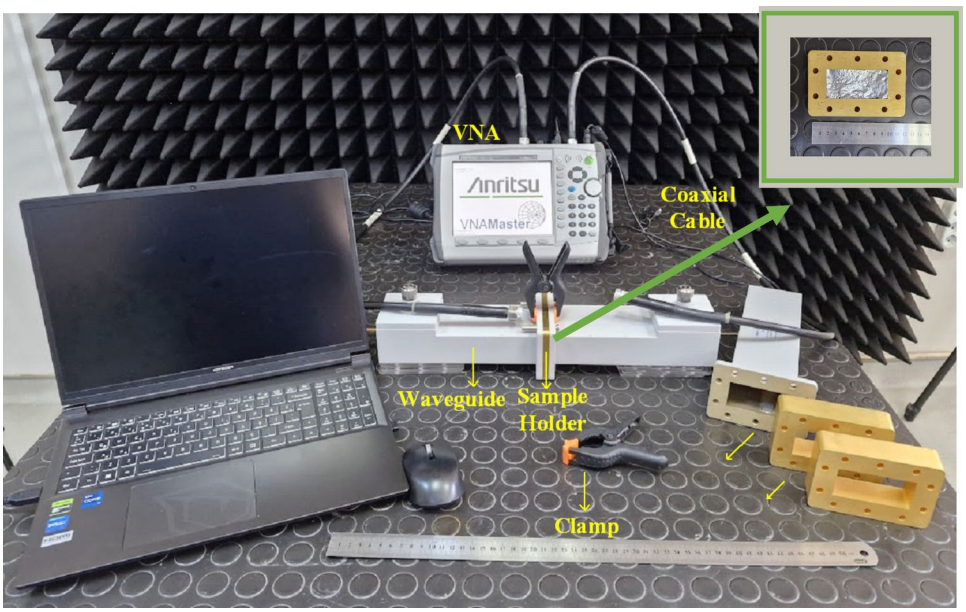

Fig. 3 Experimental configuration for EMI SE measurements. Inset: Detailed view of the TiB_2 reinforced Ag–Polymer composite

using a VNA (Fig. 3), which measured the reflection coefficient and transmission coefficient (S_{11} and S_{21}) across a frequency range of 2–4 GHz. The measurements are performed at room temperature. The experimental setup and procedure are illustrated in Fig. 2 below.

3 Results

EMI shielding performance of TiB_2-doped Ag polymer composite was systematically investigated in the 2–4 GHz frequency range. Various EM parameters, including (ε', ε''), (μ', μ''), (tan δ_e, tan δ_m), (S_{11}), (S_{21}),

and Total Shielding Effectiveness (SET), Shielding Effectiveness due to Absorption (SEA), Shielding Effectiveness due to Reflection (SER), were analyzed to comprehensively evaluate the materials' absorption and shielding mechanisms.

The X-ray diffraction (XRD) patterns of Ag polymer composite containing varying amounts of TiB_2 are presented in Fig. 4a. The pure Ag polymer composite sample exhibits broad and low-intensity peaks, indicating a predominantly amorphous structure. Upon the incorporation of TiB_2, well-defined crystalline peaks become apparent, especially for samples with 30% TiB_2 and higher. Characteristic reflections of the TiB_2 phase [(001), (100), (002), (110), (200)] are clearly observed, confirming the enhanced crystallinity and phase dominance with increasing TiB_2 content.

Additionally, the peaks corresponding to the Ag phase [(111), (200), (220), (311), (222)] are more prominent in the pure Ag polymer composite and low TiB_2 content samples. This suggests that the presence of TiB_2 may either reduce the relative intensity of the Ag phase or induce structural transformations that affect the visibility of Ag reflections. Overall, the XRD results confirm that TiB_2 significantly alters the structural characteristics of the composite by enhancing the crystalline phase contribution. Overall, the XRD analysis confirms successful incorporation of TiB_2 into Ag polymer composite matrix, with enhanced crystallinity, clear phase identification, and no significant structural incompatibility.

The average crystallite size of the samples was determined using the Debye–Scherrer equation, which relates the broadening of XRD peaks to the size of coherent diffracting domains. According to this method, smaller crystallites cause broader diffraction peaks. The equation used is

$$d(nm) = \frac{K\lambda}{B\cos\theta} \tag{6}$$

where d represents the average crystallite size, K is the shape factor (commonly taken as 0.9), λ is the wavelength of the X-ray source, B is the full width at half maximum (FWHM) of the selected diffraction peak in radians, and θ is the corresponding Bragg angle. The calculated grain size values for the samples are illustrated and compared in Fig. 4b.

The ε′ generally decreases with increasing frequency due to polarization relaxation mechanisms, as expected in typical dielectric materials. However, ε′ exhibits a strong dependence on TiB_2 content. As illustrated in Fig. 5a, composites containing 30%, 40%, and 50% TiB_2 + Ag polymer composite demonstrate significantly higher ε′ values compared to pure Ag polymer composite or powder TiB_2, especially at lower frequencies. This enhancement is attributed to interfacial polarization and the increased conductive pathways introduced by TiB_2 particles, which facilitate improved polarization response and charge transport within the matrix.

The ε″ also shows a marked increase with higher TiB_2 loading. Particularly, the 50% TiB_2 + Ag polymer composite exhibits a high ε″ value over a broad frequency band, indicating efficient attenuation of EM waves via dielectric dissipation Fig. 5b. These trends correlate directly with the dielectric loss tangent tan δ_e which maintains relatively high and stable values in composites with ≥ 30% TiB_2 content, highlighting their capacity for broadband dielectric loss.

In terms of magnetic behavior, the μ′ remains relatively close to unity for all samples Fig. 5c, indicating that the materials are not strongly magnetically active. However, μ″ is non-negligible in 30% and 40% TiB_2 + Ag polymer composites Fig. 5d, revealing those minor magnetic losses, possibly from eddy current effects and weak interfacial magnetic responses may contribute to the overall attenuation. This is supported by localized peaks in tan δ_μ, especially between 2.5–3.5 GHz in the 30–40% TiB_2 samples, which may assist in further improving impedance matching and minimizing reflection.

These combined dielectric and magnetic properties, especially the consistently high dielectric loss tangent and the presence of moderate magnetic loss promote better impedance matching with free space, enabling effective EM wave absorption. The observed enhancements beyond 30% TiB_2 content may also suggest a transition across the percolation threshold, forming continuous or semi-continuous conductive networks. This structural evolution enhances interfacial polarization and dielectric dissipation. Consequently, TiB_2 + Ag polymer composites emerge as promising candidates for broadband, thermally stable radar absorbing and shielding materials suitable for applications in aerospace and defense systems.

Figure 6a illustrates the variation of the tan δ_e with frequency for Ag polymer, powder TiB_2, and the TiB_2 + Ag polymer composites. The dielectric loss increases notably with the TiB_2 content, particularly for the composites containing 30%, 40%, and 50%

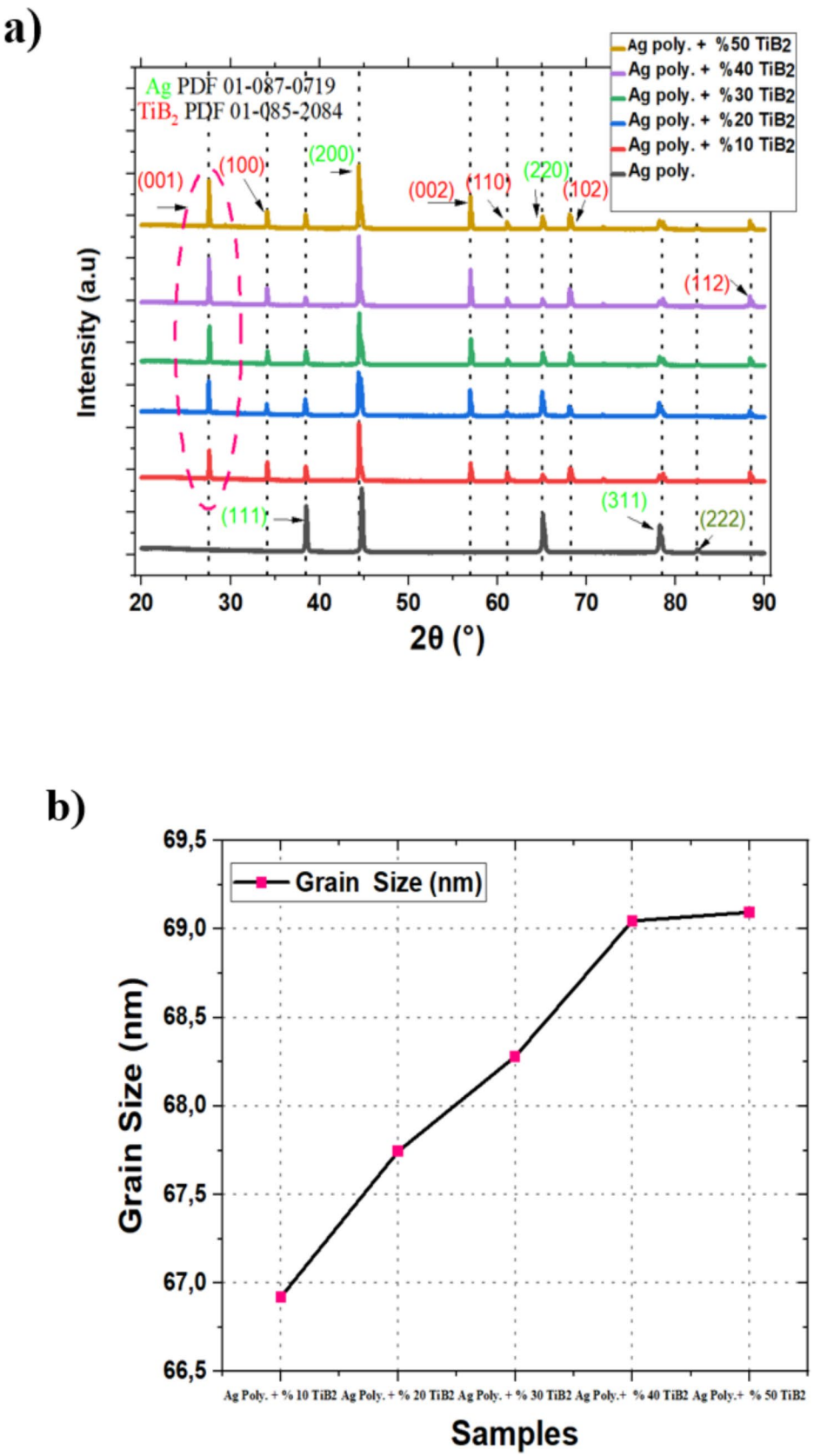

Fig. 4 **a** XRD patterns of Ag polymer composites with varying TiB_2 contents (10–50%). Diffraction peaks corresponding to TiB_2 (PDF 01–085–2084) and Ag (PDF 01–087–0719) are marked. **b** Calculated average grain size based on the Debye–Scherrer equation

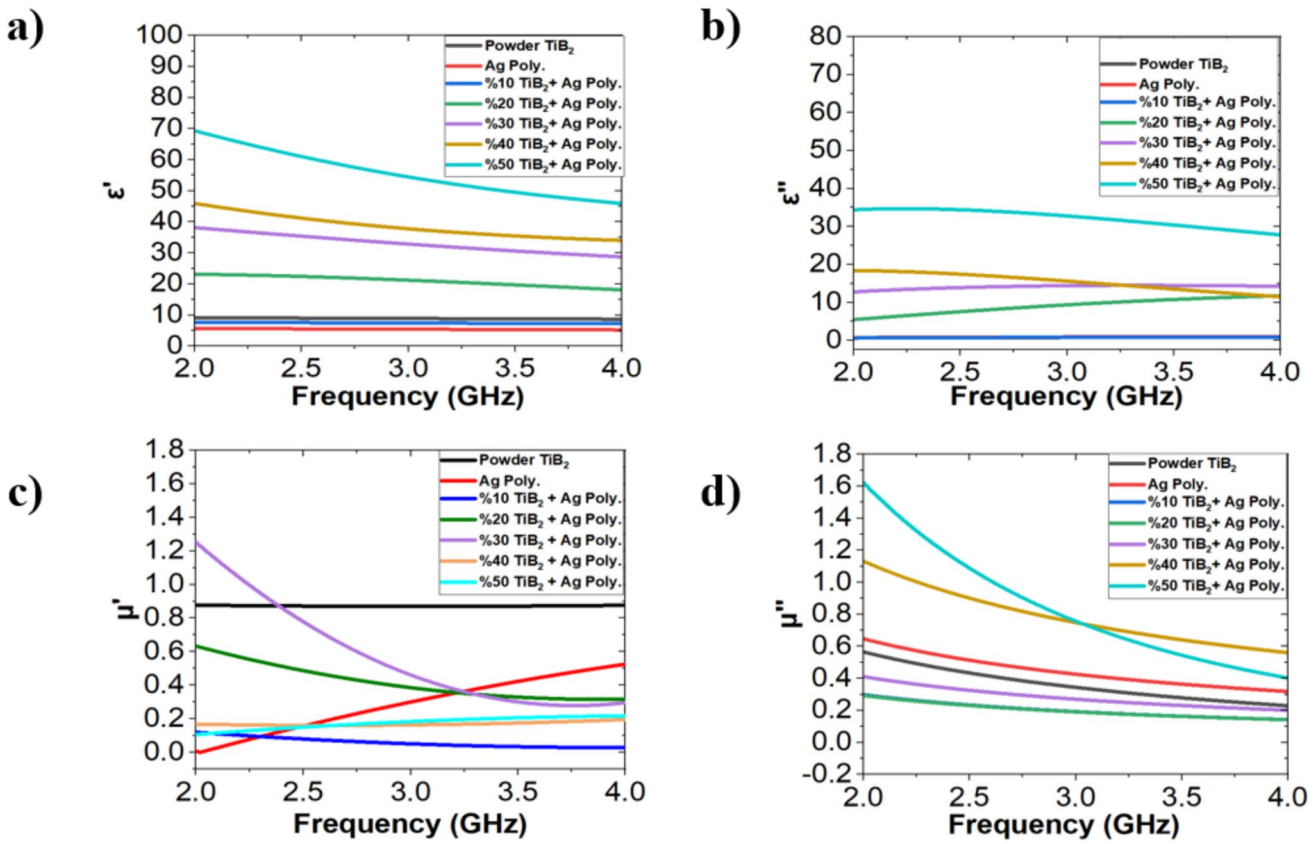

Fig. 5 **a** ε′ of the shielding material in the 2–4 GHz range. **b** ε″ indicating dielectric losses. **c** μ′ showing the magnetic response of the material. **d** μ″ associated with magnetic energy dissipation

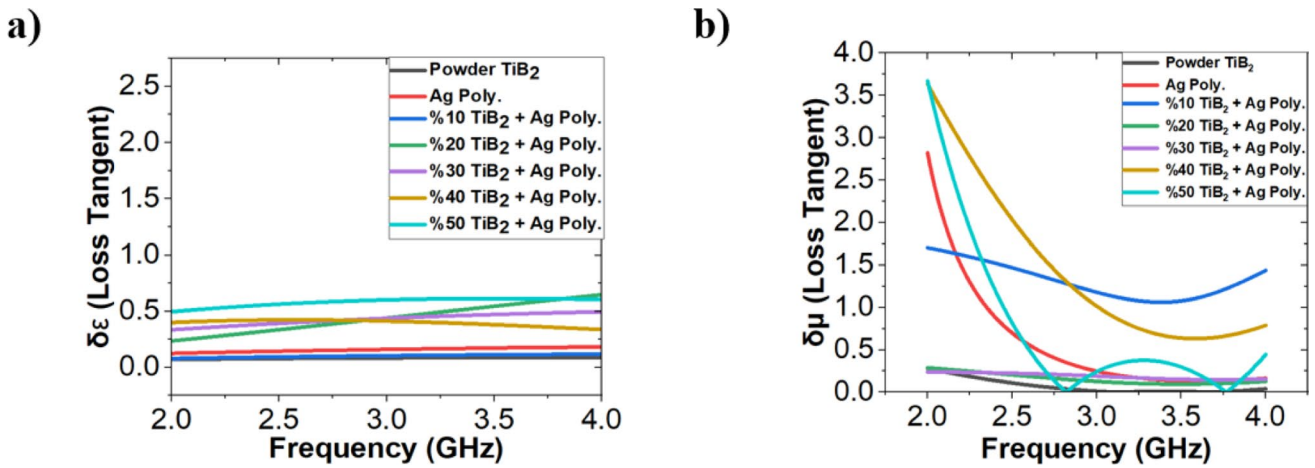

Fig. 6 **a** Tan δε of samples across the 2–4 GHz frequencyband. **b** Tan δμ of the shielding material as a function of frequency

TiB_2. These samples exhibit significantly higher tan δ_ε values compared to pure Ag polymer or powder TiB_2 across the 2–4 GHz range. The increased dielectric loss is attributed to enhanced interfacial polarization and the formation of conductive pathways within the composite matrix, which facilitate charge transport and energy dissipation through polarization mechanisms. Figure 6b displays the tan δ_μ as a function

of frequency. Pure Ag polymer and powder TiB_2 exhibit negligible magnetic losses, whereas composites with 30% and 40% TiB_2 demonstrate prominent tan δ_μ peaks, particularly between 2.5 and 3.5 GHz. These peaks suggest the presence of moderate magnetic losses, likely resulting from eddy current effects and weak interfacial magnetic responses. The 20% TiB_2 + Ag polymer composite shows a decreasing tan δ_μ trend with increasing frequency, indicating limited magnetic dissipation at higher frequencies. In contrast, the 50% TiB_2 + Ag polymer composite exhibits a relatively low and flat magnetic loss response, implying a possible saturation of magnetic effects at high filler loading levels.

Figure 7a presents the S_{11} parameters of samples as a function of frequency, serving as a key metric for evaluating microwave absorption performance. Pure Ag polymer and powder TiB_2 display poor absorption characteristics, with S_{11} values remaining above –10 dB across the measured band. In contrast, TiB_2-filled composites exhibit markedly improved performance. Notably, the 30%, 40%, and 50% TiB_2 + Ag polymer samples achieve S_{11} values below –10 dB over a broad frequency range, with minimum values approaching –15 dB near 2.1 GHz. These values indicate effective microwave attenuation, as an S_{11} value of –10 dB corresponds to 90% absorption of the incident power. Figure 7b illustrates how the S_{21} parameter of the samples varies across the frequency range. A pronounced reduction in S_{21} is observed with increasing TiB_2 content, indicating stronger attenuation through the material. Particularly, the 30% and 50% TiB_2 + Ag polymer composites demonstrate S_{21} values below –20 dB between 2.5 and 3.5 GHz, implying minimal signal transmission and suggesting that the EM energy is predominantly dissipated within the composite.

These findings confirm that increased TiB_2 loading not only enhances dielectric and magnetic losses but also improves impedance matching. The reduced reflection and transmission coefficients collectively indicate efficient absorption behavior, validating the potential of TiB_2 + Ag polymer composites as effective broadband microwave absorbers.

To gain a deeper insight into the EMI shielding mechanisms, the SET, SER, and SEA were calculated based on S-parameter measurements and are illustrated in Fig. 8a–c. As shown in Fig. 8a, the SET values demonstrate a significant enhancement with increasing TiB_2 content. The composite containing 50 wt% TiB_2 achieves peak SET values up to 45 dB, particularly within the 2.5–3.5 GHz frequency range. Similarly, the 30% and 40% TiB_2 + Ag polymer composites exhibit SET values exceeding 30 dB, which meets the industry benchmark for practical EMI shielding materials. These findings confirm that the integration of TiB_2 into the Ag polymer matrix significantly improves the overall shielding capability. Figure 8b presents the SER, which corresponds to the portion of EMI shielding resulting from surface reflection. For all samples, SER values remain relatively modest, generally below 10 dB. Although there is a slight upward trend with increasing TiB_2

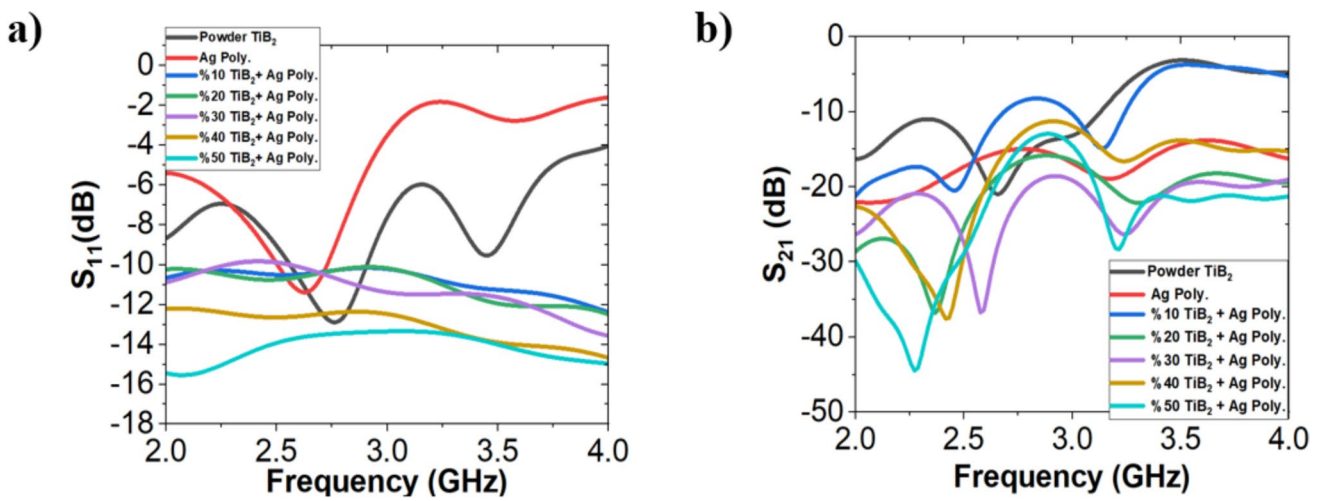

Fig. 7 **a** (S_{11}) and **b** (S_{21}) of powder TiB_2, Ag polymer, and TiB_2 + Ag polymer composites with different filler ratios in the 2–4 GHz frequency range

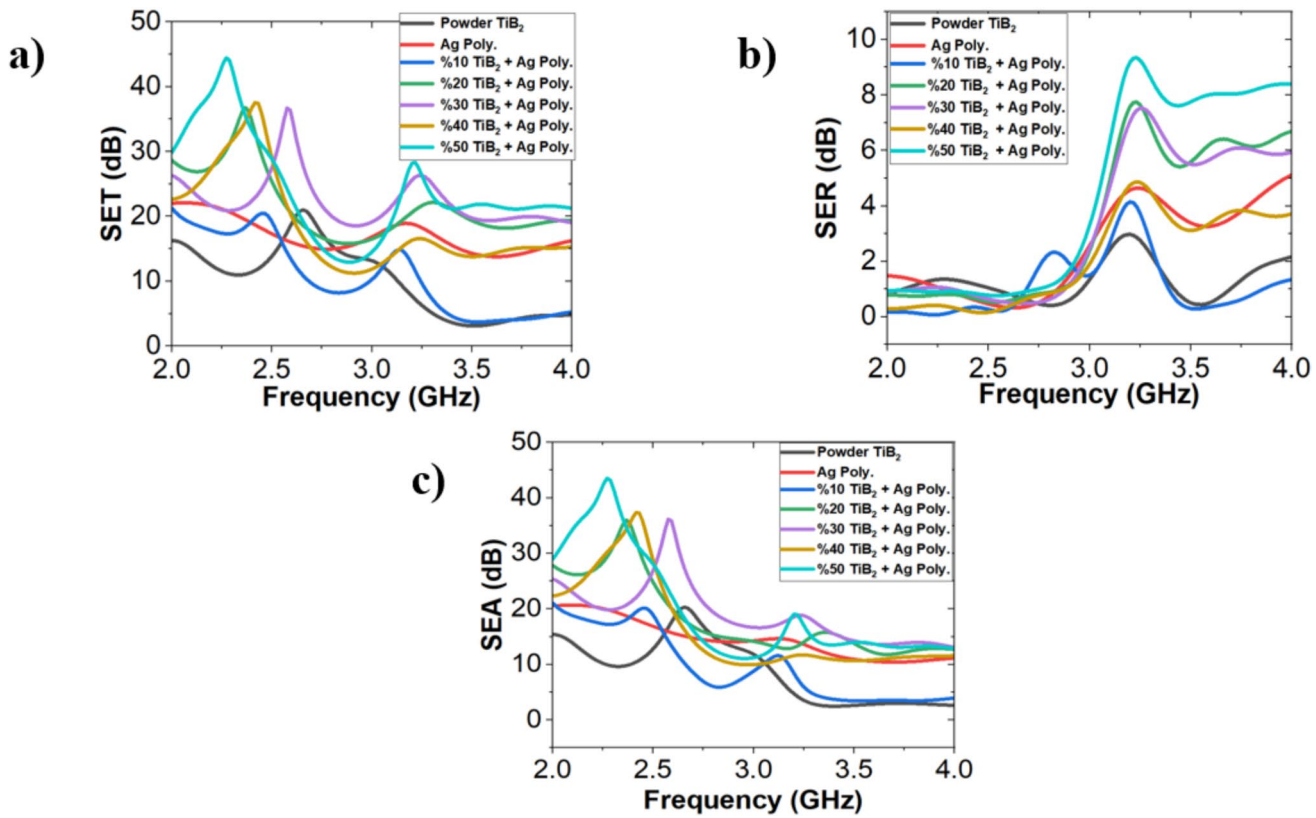

Fig. 8 **a** SET, **b** SER and **c** SEA of powder TiB_2, Ag polymer, and TiB_2 + Ag polymer composites in the 2–4 GHz frequency range

content, the reflection component is not the primary contributor to the total shielding. This implies that the surface impedance mismatch is minimal, promoting good impedance matching between the material and free space. In contrast, Fig. 8c reveals that the SEA increases prominently with higher TiB_2 concentrations and serves as the dominant shielding mechanism in nearly all samples. Notably, composites with 30% and 50% TiB_2 exhibit SEA values exceeding 30 dB over a broad frequency range. This behavior aligns well with the trends observed in the ε'' and tan δ_ε, indicating that the improved EMI shielding originates mainly from dielectric absorption processes.

Overall, the superior EMI shielding effectiveness of TiB_2-loaded composites is attributed to a synergistic combination of enhanced dielectric loss, interfacial polarization, and minor magnetic losses. These effects collectively contribute to improved impedance matching, reduced surface reflection, and increased internal absorption of incident EM radiation. Such performance confirms the potential of TiB_2 + Ag polymer composites for use in high-performance EMI shielding applications across the GHz frequency band.

4 Conclusion

This study demonstrated the potential of titanium diboride (TiB_2)-reinforced heat-resistant composite samples as effective EM shielding materials in the 2–4 GHz frequency range. By incorporating TiB_2 into a paint formulation containing an Ag-based polymer matrix at various weight fractions (10–50%), the resulting composites exhibited significant shielding effectiveness, reaching up to 45 dB at 2.2 GHz. The high attenuation observed, particularly in the reflection and transmission characteristics, confirms that TiB_2 enhances both the electrical conductivity and EM attenuation of the composite samples (Table 1).

These results suggest that TiB_2-based samples are promising candidates for applications in aerospace, defense, and high-power electronic systems, where both thermal resistance and EM shielding are critical. Further studies will focus on optimizing filler content,

Table 1 Comparison of EMI shielding effectiveness (SE) with literature

Material/Composite	Frequency (GHz)	SE (dB)	Thickness (mm)	Technique/Description	References
TiB_2-reinforced Ag polymer sample	2–4	~45	5.2	Ag-containing paint + TiB_2 composite	This study
MWNT–PVDF	1–18	~45	0.3	Solution casting + hot pressing	[20]
GNP–EVA/EOC	2–4	~20–40	~1	Melt mixing + compression molding	[21]
WS_2 nano sheets on carbon fibers	2–18	~25–40	-	Template method + pyrolysis	[22]
VO_2/CNF	1–4	52.8	1.9	–	[23]
FeSi	2–12	~30	–	Ball milling	[24]

evaluating long-term thermal stability, and extending performance across broader frequency ranges under harsh environmental conditions. The high shielding effectiveness achieved at 2.2 GHz is primarily attributed to the establishment of a robust conductive network and the reduction of skin depth within the TiB_2-Ag polymer hybrid system, showcasing its potential for next-generation.

Author contributions

TD conducted the experimental process, data collection, and measurements. ŞA contributed to the measurements and data visualization. UA was responsible for project organization and assisted in measurements. EY contributed to the organization and measurement processes. All authors reviewed and approved the final manuscript.

Funding

Open access funding provided by the Scientific and Technological Research Council of Türkiye (TÜBİTAK). This study is supported by Bursa Uludağ University Scientific Research Projects Coordination Office with projects numbered FOA-2021-630 and FPDD-2025-2206.

Data availability

The data that support the findings of this study are available from the corresponding author upon reasonable request.

Declarations

Conflict of interest The authors declare no competing interests.

References

1. Y. Li, Y. Qing, Y. Cao, F. Luo, H. Wu, Positive charge holes revealed by energy band theory in multiphase Ti_xO_{2x-1} and exploration of its microscopic electromagnetic loss mechanism. Small (2023). https://doi.org/10.1002/smll.202302769
2. Y. Gan, Y. Xiong, Review of MXene synthesis and applications in electromagnetic shielding. RSC Adv. (2025). https://doi.org/10.1039/d4ra08030k
3. S.M. Zachariah, Y. Grohens, N. Kalarikkal, S. Thomas, Hybrid materials for electromagnetic shielding: a review. Polym. Compos. (2022). https://doi.org/10.1002/pc.26595
4. X. Zhao et al., rGO aerogel embedded with organic–inorganic hybrid perovskite for lightweight broadband electromagnetic wave absorption. Nano Res. (2024). https://doi.org/10.1007/s12274-024-6880-2
5. M. González, J. Pozuelo, J. Baselga, Electromagnetic shielding materials in GHz range. Chem. Rec. **18**(7), 1000–1009 (2018). https://doi.org/10.1002/tcr.201700066
6. S. Geetha, K.K.S. Kumar, C.R.K. Rao, M. Vijayan, D.C. Trivedi, EMI shielding: methods and materials - a review. J. Appl. Polym. Sci. **112**(4), 2073–2086 (2009). https://doi.org/10.1002/app.29812
7. H. Zhang, X. Zheng, R. Jiang, Z. Liu, W. Li, X. Zhou, Research progress of functional composite electromagnetic shielding materials. Eur. Polym. J. (2023). https://doi.org/10.1016/j.eurpolymj.2023.111825
8. Y. Li et al., Unique nano porous structure derived from Co_3O_4 –C and Co/CoO–C composites towards the ultrastrong electromagnetic absorption. Compos. Part B Eng. (2021). https://doi.org/10.1016/j.compositesb.2021.108731
9. Y. Li et al., Ceramic-based electromagnetic interference shielding materials: mechanisms, optimization strategies, and pathways to next-generation applications. J. Adv. Ceram. (2025). https://doi.org/10.26599/jac.2025.9221194
10. K.S. Kumar, R. Rengaraj, G.R. Venkatakrishnan, A. Chandramohan, Polymeric materials for electromagnetic shielding - a review. Mater. Today Proc. **45**, 4925–4928 (2021). https://doi.org/10.1016/j.matpr.2021.03.720
11. S. Zheng, Y. Wang, X. Wang, H. Lu, Research progress on high-performance electromagnetic interference shielding materials with well-organized multilayered structures. Mater. Today Phys. (2024). https://doi.org/10.1016/j.mtphys.2024.101330
12. Y. Liu et al., A highly deficient medium-entropy perovskite ceramic for electromagnetic interference shielding under harsh environment. Adv. Mater. (2024). https://doi.org/10.1002/adma.202400059
13. A.A.A. Sanad, M.N. Mahmud, M.F. Ain, M.A.B. Ahmad, N.Z.B. Yahaya, Z.M. Ariff, Theory, modeling, measurement, and testing of electromagnetic absorbers: a review. Phys. Status Solidi A (2024). https://doi.org/10.1002/pssa.202300828
14. B. Dai et al., Overview of MXene and conducting polymer matrix composites for electromagnetic wave absorption. Adv. Compos. Hybrid Mater. **5**(2), 704–754 (2022). https://doi.org/10.1007/s42114-022-00510-6
15. G. Jandieri, D. Sakhvadze, Controlled synthesis of TiB_2 -TiC composite: substantiation of the homogenizing Joule thermostatting efficiency and improvement of SHS-compaction technology in a vacuum. J. Eng. Sci. **11**(2), C13–C28 (2024). https://doi.org/10.21272/jes.2024.11(2).c2
16. Z. Song, M. Sun, L. Wu, F. Wu, A. Xie, Dielectric loss behavior and microwaves absorption properties of TiB2 ceramic. Mater. Res. Express (2020). https://doi.org/10.1088/2053-1591/ab85fb
17. Y. Li, Y. Qing, Y. Zhang, H. Xu, Simultaneously tuning structural defects and crystal phase in accordion-like TixO2x-1 derived from Ti3C2Tx MXene for enhanced electromagnetic attenuation. J. Adv. Ceram. **12**(10), 1946–1960 (2023). https://doi.org/10.26599/JAC.2023.9220799
18. K. Hirako et al., Development of small satellite for X-Band compact synthetic aperture radar. J. Phys. Conf. Ser. **1130**(1), 012013 (2018). https://doi.org/10.1088/1742-6596/1130/1/012013
19. E.G.B. Dassan, A.A.A. Rahman, M.S.Z. Abidin, H.M. Akil, Carbon nanotube-reinforced polymer composite for electromagnetic interference application: a review. Nanotechnol. Rev. **9**(1), 1068–1088 (2020). https://doi.org/10.1515/ntrev-2020-0064
20. G.S. Kumar, D. Vishnupriya, A. Joshi, S. Datar, T.U. Patro, Electromagnetic interference shielding in 1–18 GHz frequency and electrical property correlations in poly(vinylidene fluoride)–multi-walled carbon nanotube composites. Phys. Chem. Chem. Phys. **17**(1), 110–158 (2015). https://doi.org/10.1039/C5CP02585K
21. F. Pontes, B.G. Soares, Effect of graphite nanoplatelets on the electromagnetic shielding effectiveness of EVA/EOC blends. Compos. Sci. Technol. **212**, 108716 (2021). https://doi.org/10.1016/j.compscitech.2021.108716
22. H. Zhang et al., Engineering flexible and green electromagnetic interference shielding materials with high performance through modulating WS2 nanosheets on carbon fibers. J. Materiomics **8**(2), 327–334 (2022). https://doi.org/10.1016/j.jmat.2021.09.003
23. S.Y. Liao et al., Intelligent shielding material based on VO_2 with tunable near-field and far-field electromagnetic

response. Chem. Eng. J. (2023). https://doi.org/10.1016/j.cej.2023.142596

24. Y. Xu, L. Yuan, J. Cai, J. Lv, D. Zhang, Effects of particle sizes on the electromagnetic property of flaky FeSi composites. Acta Metall. Sin. (Engl. Lett.) **26**(4), 366–372 (2013). https://doi.org/10.1007/s40195-013-0003-5